MDPI

Article

Source and Migration Pathways of Heavy Metals in Soils from an Iron Mine in Baotou City, China

Changyu Wang [1,2], Danhong Xu [3,4], Yongli Li [1,2,*], Wenhui Zhou [1,2], Peng Bian [1,2] and Siyuan Zhang [1,2]

1   Hohhot General Survey of Natural Resources Center, China Geological Survey, Hohhot 010010, China; cgstjwchangyu@126.com (C.W.); zhouwenhui@mail.cgs.gov.cn (W.Z.); bianpeng@mail.cgs.gov.cn (P.B.); zhangsiyuan@mail.cgs.gov.cn (S.Z.)
2   Innovation Base for Water Resource Exploration and Eco-Environmental Effects in the Daheihe Basin of the Yellow River, Hohhot 010010, China
3   Tianjin Center, China Geological Survey, Tianjin 300170, China; s454650073@126.com
4   North China Center of Geoscience Innovation, Tianjin 300170, China
*   Correspondence: lyongli@mail.cgs.gov.cn; Tel.: +86-15248185113

Abstract: The exploitation of iron ore could cause heavy metals pollution in the soils, which threatens the ecosystem and human health. In this study, soil, stream sediment, tailings, rock, and atmospheric deposition samples were collected from an iron mine in Baotou City. The concentrations of As, Cd, Cr, Cu, Hg, Ni, Pb, Zn, Al_2O_3, CaO, K_2O, MgO, Na_2O, SiO_2, and Fe_2O_3, as well as the mineral composition and heavy metal speciation of the samples, were analyzed for pollution assessment and source identification of heavy metals. The results reveal that the concentration of Cu in the soils was significantly higher than the background value, and an unpolluted to moderately polluted state was the main pollution level. By analyzing the relationship between Cu/Al_2O_3 and CaO in different samples, as well as the characteristics of the chemical index of alteration (CIA), mineral composition, and the chemical speciation of Cu in soils and profiles, the results suggest that tailings were the source of Cu pollution in soils. The distribution characteristics of Cu and CaO in stream sediments indicated that hydraulic transport may be one of the main migration pathways. In addition, wind transport may also be a pathway of migration.

1. Introduction

With the exploitation of mineral resources, the economy is developing rapidly, but ecological and environmental problems are also increasing [1,2]. Owing to the insufficient awareness of environmental protection, a plethora of issues have arisen in mining areas, encompassing geological disasters, ecological degradation, and environmental contamination [3–5]. The exploitation of mineral resources generates various types of waste, which often contains high levels of heavy metals. The improper treatment of accumulation and discharge can lead to serious pollution of the water and soils in the mining area [6–9]. At present, land area contaminated by mining in China exceeds 2 million hectares and is increasing at a rate of 33,000–47,000 hectares per year [10]. Heavy metals in soil have prolonged residual periods and pose significant biological toxicity to animals, plants, and microorganisms. This toxicity can result in damage to the ecosystem [11–13]. They can also migrate to the human body through ingestion, inhalation, skin exposure, and food chains, posing a threat to people's health [14–19]. Cd might cause Minamata disease, Hg might cause itai-itai disease, and Cu might cause cardiovascular disease, retinal disease, and cancer [20,21].

The source of heavy metals mainly refers to where the pollution elements mainly come from. It mainly includes two types. One is derived from rock weathering, and the other is

from external input, mainly affected by human activities, such as agriculture, industry, and life [22–24]. The migration pathways of heavy metals refer to how the pollution elements migrate from the source to the soil. And they can be mainly classified into physical and chemical migration [25]. Chemical migration refers to the migration of elements through dissolution [26]. Physical migration is mainly the migration of elements with the transport of detritus, including hydraulic transport and wind transport [25,27]. Research on the combination characteristics of elements, such as correlation and principal component analysis, can identify the possible source of heavy metals and the contribution rate of each source according to the combination characteristics of elements [28–31]. However, the study of migration pathways requires being combined with other methods. Isotopes are often used in traceability research. For example, Pb isotopes have a good effect on the tracing of Pb [32–34]. In recent years, more isotopes have been used in the traceability research of elements [35–37]. But the test sample contains additional elements that will cause polyatomic interference during the isotope test. Currently, there is still no established technology to effectively separate and purify the samples in order to eliminate these elements [38]. Additionally, the current research on isotope fractionation of contaminants is also in its early stages. Therefore, accurate tracing of all heavy metals using isotopes may not be feasible [39,40]. The geochemical speciation of heavy metals can also be used to identify the source of heavy metals. In the soils weathered from the parent rocks, most of the heavy metals mainly exist in the stable-state form, while the active state is mainly affected by human activities [41,42], but this feature is not fixed [43]. A single method often has certain limitations, so it is best to use a variety of methods to confirm the others.

Baotou City is located in a semiarid area, and its ecosystem is fragile. Once the soils are polluted, they are difficult to restore [44]. There are a large number of metal minerals and rare-earth minerals, especially iron ore, which are widely distributed in the study area and have a high yield [45]. The mining, mineral processing, smelting, and tailings stacking of iron ore have caused heavy metal pollution in the surrounding topsoils [46,47].

In recent years, China has promulgated a series of plans, systems, and standards to ensure the implementation of mine ecological restoration projects [48]. Soil pollution remediation is a very important work in mine ecological restoration. This study aims to control soil pollution from the source by studying the source and migration pathways of heavy metals. This can support the environmental protection and restoration of soils in mining areas. In this study, soil, stream sediment, tailings, rock, and atmospheric deposition samples were collected. The concentrations of As, Cd, Cr, Cu, Hg, Ni, Pb, Zn, Al_2O_3, CaO, K_2O, MgO, Na_2O, SiO_2, and Fe_2O_3 were measured, and the mineral composition and chemical speciation of heavy metals of samples were tested. The specific objectives of this study are (1) to determine the concentration and pollution level of heavy metals in the soils of the study area; (2) to analyze the main sources of heavy metals in the soils of the study area; (3) and to analyze the main migration pathways of heavy metals.

2. Materials and Methods

2.1. Overview of Study Area

As Figure 1a shows, the study area is situated in Baotou City (110°12′~110°19′ E, 40°58′~41°03′ N), and located in the Guyang–Jining fracture on the northern margin of the North China Platform, which belongs to the Yinshan metamorphic area [49]. The Neoarchean Se'ertengshan group, the Mesoproterozoic Zhaertaishan group, and the quaternary are outcropping in the study area. The intrusive rocks include the Dajitu rock mass and the Wengeqi rock mass [50]. The rocks mainly include biotite plagioclase gneiss, quartz diorite, dolomite, and diopside amphibolite. The study area belongs to a temperate continental climate, with an average temperature of 8.4 °C and a precipitation of 240.4 mm in 2021 (Baotou Statistical Yearbook, 2022). The interannual variation range of precipitation-weighted pH in the Baotou urban area from 2017 to 2021 was 6.39 to 7.28, with an average value of 6.86 [51]. The southeast wind prevails in summer and the northwest wind prevails in winter. The iron mine in the study area is currently in production, and the mode of

mining is open-pit. There are ore-dressing plants, tailings reservoirs, and tailings dumps distributed around the mine.
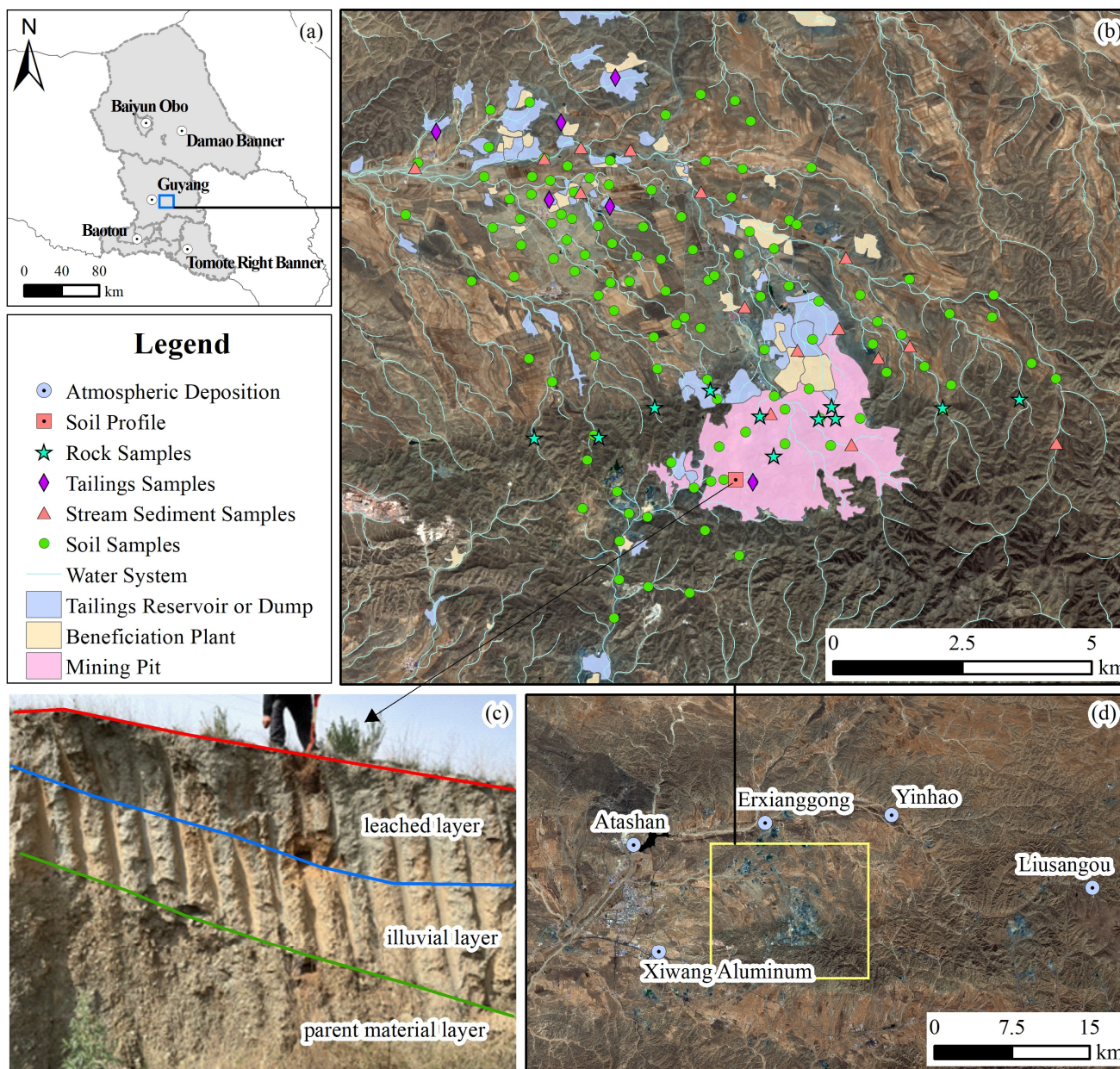

Figure 1. (**a**) Location map of study area; (**b**) the distribution of soil, tailing, stream sediment, rock samples, and soil profile (background of the raster image: Sentinel-2 satellite image); (**c**) photo of the soil profile; (**d**) distribution of the atmospheric site (background of the raster image: Sentinel-2 satellite image).

2.2. Sample Collection and Processing

2.2.1. Soil Sample

In order to assess heavy metal pollution, 113 soil samples were collected from the study area from August to September 2021. The distribution of soil samples is presented in Figure 1b. Overall, the distribution of soil samples in the study area was uniform. The samples were collected at a depth of 0~20 cm. Each sample consisted of a primary point and four secondary points, which were positioned around the primary point within a distance range of 15 to 20 m, forming an 'X' shape. We recorded the coordinates of the major point after sampling. The samples were placed in cotton cloth bags and hung

on the rack for natural drying. Dried samples were filtered through a 10-mesh (2 mm) nylon sieve. Following screening, 500 g of sieved samples was put into a polystyrene plastic bottle using the quartering method and sent to the laboratory for geochemical and mineralogical analysis.

2.2.2. Tailings and Rock Sample

A total of 6 tailings and 12 rock samples were collected to identify the source of soil heavy metal pollution, and the sample sites are presented in Figure 1b. Tailings samples were collected in the tailings reservoir or dump, and the sampling and processing methods of tailings were the same as soil. Rock samples were collected from different strata and rock masses based on the geological map and the survey in situ observation. After collection, the rock samples were sent to laboratory for rock identification and crushed into 200-mesh for geochemical analysis.

2.2.3. Soil Profile Sample

In order to analyze the natural weathering process and human influence on the surface soil, the soil profile was collected. The photo of the soil profile is presented in Figure 1c. Soil samples in leached layer (PM-A, 0~20 cm), illuvial layer (PM-B, 80~100 cm), and parent material layer (PM-C, 200–220 cm) were collected in July 2022. The soil profile was formed by in situ weathering of rocks, and there was a tailings dump 100 m upstream of the southeast side of the soil profile. Therefore, the concentrations of elements in the topsoil of this profile might be affected by both weathering and human influence.

2.2.4. Stream Sediment and Atmospheric Deposition Sample

Fifteen stream sediment samples were collected from the riverbed of seasonal rivers and gullies in the study area, and the distribution of samples is presented in Figure 1b; the major flow direction was from southeast to northwest. Each stream sediment sample was mixed with three subsamples. After drying, the stream sediment samples were sieved to a range of 20~4 mesh (0.85~4.75 mm), which mainly represented debris rather than soil. Five atmospheric deposition samples were collected from the residential areas in different wind directions in the study area, and the atmospheric deposition sites are presented in Figure 1d. The purpose was to collect rain and dust in the study area from October 2020 to October 2021. During the sample collection period, a plastic bucket that was washed with distilled water was positioned on the roof of the resident's house, approximately 3–5 m away from the chimney. Following collection, the bucket was retrieved, sealed, and then transported to the laboratory for geochemical analysis.

2.3. Analytical Methods

The samples must be ground to a 200 mesh (0.075 mm) in the laboratory for the purpose of analyzing element concentration, mineral composition, and heavy metal speciation. Heavy metals in rocks may exist within silicate minerals (with representative elements Al_2O_3, SiO_2, Fe_2O_3, and so on) due to isomorphism, while heavy metals in soil may be adsorbed by clay minerals (with representative elements Al_2O_3, SiO_2, Fe_2O_3, MgO, and so on) [52]. This suggests that the concentration of heavy metals is closely related to the concentration of major elements. Therefore, As, Cd, Cr, Cu, Hg, Ni, Pb, Zn, Al_2O_3, CaO, K_2O, MgO, Na_2O, SiO_2, and Fe_2O_3 were measured. In the laboratory, crushed samples were made into thin sections at a pressure of 30 MPa to measure SiO_2, Fe_2O_3, Al_2O_3, Cr, Pb, Zn, K_2O, MgO, Na_2O, and CaO with X fluorescence spectrometer (XFS, ADVANT'X Series, USA), digested with mixed acids ($HClO_3$, HNO_3, and HCl) at approximately 240 °C to determine Cd, Cu, Ni with inductively coupled plasma mass spectrometry (ICP-MS, Agilent 7700X, USA), and also digested with aqua regia at 95~98 °C to determine As and Hg with atomic fluorescence spectrometer (AFS, AFS-3000, China). The standard materials (GBW) of GBW07401, GBW07402, GBW07403, GBW07404, GBW07405, GBW07407, GBW07408, GBW07423, GBW074010, GBW074012, GBW07303, and GBW07304 were measured during

the sample measurement for quality control. The detection limits of elements are presented in Table 1. Prior to conducting the sample test, the standard materials (GBW) underwent measurements 12 times. The logarithmic deviations (ΔlgC_{GBW}) between the measured value (C_i) and the standard value (C_s) of standard materials were calculated for each analysis result of each element. The requirements for logarithmic deviations are outlined in Table 2. The accuracy qualification rate of each element should be greater than or equal to 98%. For each set of 50 samples, 4 standard materials were measured. The logarithmic standard deviation (λ) of each standard material was calculated, and the requirement for precision is presented in Table 2. The analytical data in this study meet the quality requirements.

Table 1. The detection limits of elements.

Element	Detection Limit	Element	Detection Limit
As	0.5	SiO_2	0.1 *
Cd	0.03	Al_2O_3	0.05 *
Cr	2.5	Fe_2O_3	0.05 *
Cu	1	K_2O	0.05 *
Hg	0.0005	Na_2O	0.05 *
Ni	2	CaO	0.05 *
Pb	2	MgO	0.05 *
Zn	4		

* Unit: %. Unit of other elements: $mg \cdot kg^{-1}$.

Table 2. The methods of calculation and the criteria for accuracy and precision (ΔlgC_{GBW}, logarithmic deviation; C_i, measured value of standard materials; C_s, standard value of standard materials; λ, logarithmic standard deviation).

Range of Concentration	Accuracy (Calculation method: $\Delta lgC_{GBW} = |lgC_i - lgC_s|$)	Precision (Calculation method: $\lambda = \sqrt{\frac{\sum_{i=1}^{n}(lgC_i - lgC_s)^2}{4-1}}$)
Within 3 times detection limit	≤ 0.12	≤ 0.17
Exceeding 3 times detection limit	≤ 0.10	≤ 0.15
1%~5%	≤ 0.07	≤ 0.10
>5%	≤ 0.05	≤ 0.08

Heavy metal speciations were measured according to the seven-step continuous extraction method proposed by the China Geological Survey [53], which is presented in Table 3.

The geochemical stability of major elements is significantly influenced by the mineral phases, and the concentration of elements is related to the proportion of each mineral in the samples. So, the whole rock mineral composition of samples was analyzed. The ground powder samples were loaded into the sample stage of the X-ray diffractometer (XRD) and then compacted with a smooth, flat glass. The diffraction peak intensity was analyzed using an X-ray diffractometer (Malvern Panalytical Empyrean series 2, Malvern Panalytical, Malvern, UK) with a Cu target, 40 kV voltage, and 40 mA current. The scanning range spans from 5° to 70° (2θ), with a step width of 0.013° (2θ). The mineral phase characteristics were analyzed using Jade 6.5 software, and the Rietveld full-spectrum fitting method was employed for semiquantitative analysis of mineral content [54]. The content of each individual mineral is expressed as its proportion in the whole rock mineral.

Table 3. Sequential extraction procedures.

Step		Extractant	Operating Procedure
F1	Water-soluble fraction	distilled water	Take 25 mL, shake, oscillate for 30 min, centrifuge for 20 min, and filter.
F2	Exchangeable fraction	1 mol·L^{-1} magnesium chloride solution	Take 25 mL, shake, oscillate for 30 min, centrifuge for 20 min, and filter.
F3	Carbonate bonding fraction	1 mol·L^{-1} sodium acetate solution	Take 25 mL, shake, oscillate for 1 h, centrifuge for 20 min, and filter.
F4	Humic acid bonding fraction	0.1 mol·L^{-1} sodium pyrophosphate solution	Take 50 mL, shake, oscillate for 40 min, wait 2 h, centrifuge for 20 min, and filter.
F5	Fe-Mn oxidation fraction	0.25 mol·L^{-1} mixture of hydroxyamine hydrochloride and hydrochloric acid	Take 50 mL, shake, oscillate for 1 h, centrifuge for 20 min, and filter.
F6	Organic bonding fraction	30% hydrogen peroxide, (1 + 1) nitric acid solution, 3.2 mol·L^{-1} ammonium acetate–nitric acid mixture	Take 3 mL HNO$_3$ and 5 mL H$_2$O$_2$, shake, then bathe in a constant-temperature water bath for 1.5 h, add 3 mL H$_2$O$_2$, and bathe in the water bath for 70 min. Finally, add 2.5 mL of the ammonium acetate–nitric acid solution, dilute to 25 mL and leave for 10 h, centrifuge for 20 min, and filter.
F7	Residual fraction	-	Step F6 leftover residue is air-dried, finely powdered, and weighed.

2.4. Statistical Method

SPSS Statistics 19 software was used to calculate the minimum (Min), maximum (Max), average (Mean), and standard deviation (SD) of element concentration in different samples. The coefficient of variation (CV) was determined using the following Equation (1):

$$CV = SD/Mean \times 100\% \tag{1}$$

It is generally recognized that a CV ≤ 16% is considered as weak variation, 16% < CV < 36% is considered as moderate variation, and a CV ≥ 36% is considered as strong variation [55].

2.5. Enrichment Factor

This study defined the enrichment factor (EF) as the ratio of the average concentration of elements to the geochemical background value. The calculation formula is presented in Equation (2).

$$EF = \overline{C_n}/B_n \tag{2}$$

where $\overline{C_n}$ is average concentration of elements, and B_n is the local soil background values in soil. In this paper, the background value of surface soil in the Hetao Plain was chosen as the local soil background value. It represents the average concentration of elements on the alluvial plain in the piedmont of Yinshan Mountain [56].

2.6. Geoaccumulation Index

The geoaccumulation index (I_{geo}) was first developed by Muller and is used to assess different pollution levels in bottom sediments and soils [57–59]. The geoaccumulation index was calculated from the following Equation (3):

$$I_{geo} = \log_2[C_n/1.5B_n] \tag{3}$$

where C_n is the concentration of each heavy metal in the soils, and B_n is the local soil background values of each heavy metal. On the basis of the geoaccumulation index, the level of pollution of the soils can be classified into six different classes (Table 4) [57].

Table 4. Geoaccumulation index classification and pollution intensity.

I_{geo}-Class	Geoaccumulation Index	Pollution Intensity
6	>5	Very strong pollution
5	>4–5	Strong to very strong
4	>3–4	Strongly polluted
3	>2–3	Moderately to strongly
2	>1–2	Moderately polluted
1	>0–1	Unpolluted to moderate
0	<0	Practically unpolluted

2.7. Chemical Index of Alteration

The chemical index of alteration (CIA) is commonly used to assess the degree of chemical weathering in the source area [60]. And it was calculated using Equation (4):

$$CIA = \{\omega(Al_2O_3)/[\omega(Al_2O_3) + \omega(CaO^*) + \omega(Na_2O) + \omega(K_2O)]\} \times 100 \qquad (4)$$

where $\omega(Al_2O_3)$, $\omega(Na_2O)$, and $\omega(K_2O)$ represent the molar fractions of Al_2O_3, Na_2O, and K_2O, while $\omega(CaO^*)$ refers to the molar fraction of CaO in silicate [61].

3. Results

3.1. Characterization of Heavy Metal and Major Element

The statistical results of the concentration of heavy metals in the soils, tailings, and stream sediments are presented in Table 5. In the soils, the average concentration of As, Cd, Hg, and Pb was found to be lower than the local soil background values. While that of other heavy metals was higher than the background values, and the enrichment factor of Cu, Cr, Ni, and Zn was 2.6, 1.4, 1.4, and 1.05. The average concentration of Cu in the tailings and stream sediments was also higher than the background value. In the tailings, the enrichment factor of Cu was 16.28. Compared with the "National Soil Environmental Quality Standards" (GB15618-2018) [62], 13 soil samples, 6 tailings samples, and 1 stream sediment sample exceeded the risk screening value for Cu. There was also one soil and one tailings sample exceeding the risk screening value for Cr. In the soil, the coefficient of variation (CV) of heavy metals followed the order of Cu >Ni > Cr > Hg > Zn > Cd > As > Pb. The CV of Cu, Ni, Cr, and Hg were all higher than 36%, indicating strong variability. Table 6 presents the concentration of heavy metals in the rocks. The results reveal that the concentration of Cu ranged from 5 to 124 mg·kg^{-1}, with the highest concentration found in diopside rock, which contained iron ore. The risk screening value for Cu was only exceeded in the ore-bearing rock.

The statistical results of the concentration of major elements in the soils, tailings, and stream sediments are also presented in Table 5. In the soils, the average concentration of Al_2O_3, CaO, Fe_2O_3, MgO, and Na_2O was higher than the background values. The maximum concentration of CaO was 2.9 times the background values, and the enrichment factor was 1.02. In the tailings, the average concentration of CaO, Fe_2O_3, and MgO was significantly higher than the background value. The concentration of CaO ranged from 14.24 to 20.43%, with an enrichment factor of 3. In the stream sediments, the average concentration of Al_2O_3, Fe_2O_3, K_2O, MgO, and Na_2O was higher than the background values. The concentration of Na_2O and K_2O in the stream sediments was also higher than that in the soils and tailings. The CV of major elements in tailings was all less than 36%, while the CV of CaO, and MgO was more than 36% in soils and stream sediments, which belong to strong variability. The concentration of major elements in the rocks is presented

in Table 6. The results reveal that the concentration of CaO in diopside rock was generally higher, ranging from 18.09% to 21.22 %.

Table 5. Statistical results of the concentration of heavy metals and major elements in the soils, tailings, and stream sediments (unit of heavy metals: mg·kg^{-1}; unit of major elements: %).

		As	Cd	Cr	Cu	Hg	Ni	Pb	Zn	Al$_2$O$_3$	CaO	Fe$_2$O$_3$	K$_2$O	MgO	Na$_2$O	SiO$_2$
Soils	Min	1.8	0.05	34.5	15	0.004	14	7	24	7.27	2.02	2.30	1.69	1.30	0.63	45.8
	Max	15.3	0.30	352.0	378	0.058	114	33	153	14.98	16.88	12.16	3.08	11.64	3.15	70.7
	Mean	7.7	0.10	78.8	49	0.019	34	16	59	11.30	5.99	5.10	2.16	2.89	2.19	61.2
	SD	2.3	0.04	37.4	53	0.007	17	3	20	1.11	2.58	1.56	0.23	1.56	0.37	3.9
	CV(%)	29.3	33.8	47.5	107.9	38.5	49.2	20.0	34.6	9.9	43.1	30.6	10.7	54.1	17.1	6.3
Tailings	Min	1.4	0.14	52.7	265	0.005	43	3	90	5.63	14.24	8.37	0.77	8.06	0.65	43.3
	Max	2.8	0.20	345.0	341	0.010	120	9	209	9.03	20.43	15.36	1.79	11.37	1.36	50.8
	Mean	2.1	0.17	120.0	312	0.006	64	5	133	7.02	17.65	10.51	1.18	10.10	0.90	47.2
	SD	0.4	0.03	111.0	28	0.002	29	2	54	1.51	2.64	2.75	0.39	1.17	0.26	2.6
	CV(%)	22.4	16.4	92.8	9.1	29.4	44.9	39.0	40.1	21.5	15.0	26.1	32.8	11.5	28.5	5.5
Stream sediments	Min	0.9	0.04	58.4	13	2.292	17	10	35	9.75	2.59	2.79	2.35	1.27	1.69	50.6
	Max	3.8	0.10	133.2	169	5.750	49	16	92	14.91	8.58	8.50	3.99	7.61	4.75	62.0
	Mean	2.0	0.06	86.6	39	0.004	30	12	56	13.08	4.72	4.90	3.22	2.98	3.54	57.7
	SD	1.0	0.02	24.1	38	1.162	10	2	15	1.53	2.06	1.60	0.48	2.00	1.14	3.2
	CV(%)	47.1	29.8	27.8	98.4	32.8	32.5	16.4	26.6	11.7	43.7	32.7	14.9	67.2	32.3	5.5
Background values [1]		9.7	0.12	56.4	19	0.025	25	19	56	11.03	5.89	3.62	2.26	1.91	1.92	65.13
Risk screening values [2]		20	0.6	250	100	3.4	190	170	300	-	-	-	-	-	-	-

[1] Data cited in Reference [56]; [2] Data cited in Reference [62].

Table 6. The concentration of heavy metals and major elements in the rocks (unit of heavy metals: mg·kg^{-1}; unit of major elements:%).

Sample	Rock Identification	As	Ni	Cu	Pb	Cr	Al$_2$O$_3$	CaO	Fe$_2$O$_3$	K$_2$O	MgO	Na$_2$O	SiO$_2$
YS04	diorite	1.9	14	36	10	33	15.33	3.06	2.20	1.39	4.95	1.44	68.00
YS05	diorite	1.1	65	45	7	221	14.74	4.36	2.47	1.56	4.02	3.98	60.88
YS06	leptynite	4.4	51	24	19	111	14.24	3.79	4.90	3.54	3.02	3.13	59.40
YS07	marble	6.5	2	24	5	10	0.77	36.46	0.37	0.26	0.08	14.86	16.76
YS08	diopside rock	0.9	53	5	3	111	5.75	18.24	4.65	2.23	0.74	13.49	46.53
YS09	diopside rock	0.9	68	11	3	81	5.15	18.09	13.20	1.14	0.74	9.06	36.99
YS10	monzonite	0.3	530	25	9	977	10.54	7.17	2.89	2.71	2.30	12.65	49.73
YS11	diorite	0.4	26	45	20	75	17.90	4.77	2.96	3.32	4.66	2.90	56.67
YS12	diopside rock (ore-bearing)	1.2	45	124	4	76	2.39	21.22	12.25	0.38	0.36	11.18	38.14
YS13	monzonite	0.7	25	38	14	92	15.56	5.87	3.74	3.03	3.70	4.34	55.36
YS14	diorite	0.4	66	28	18	187	16.02	4.06	2.62	4.21	3.06	4.29	59.03

3.2. Heavy Metals Pollution Assessment

The results of the geoaccumulation index (I$_{geo}$) of heavy metals in the soils are presented in Figure 2. The average of I$_{geo}$ was in the order of Cu (0.37) > Cr (−0.19) > Ni (−0.22) > Zn (−0.58) > Pb (−0.81) > Cd (−0.82) > As (−1.00) > Hg (−1.11). Apart from Cu, the average I$_{geo}$ of heavy metals was less than 0. This suggested that there was obvious contamination of Cu in the soils, while As, Cd, Cr, Hg, Ni, Pb, and Zn were mainly in a practically unpolluted state. The proportion of samples in the unpolluted to moderately polluted state for As, Cd, Cr, Hg, Ni, Pb, and Zn was 0.9%, 4.4%, 21.2%, 0.9%, 23%, 0.9%. There were three (2.7%) samples in a moderately polluted state and one (0.9%) sample in a moderately to strongly polluted state for Cr. And there were also four (3.5%) samples in a moderately polluted state for Ni. The I$_{geo}$ of Cu ranged from −0.92 to 3.72. There were 65 polluted samples, accounting for 57.5% of the samples. The unpolluted to moderately polluted state was the predominant pollution level, accounting for 36.3% of samples. The proportion of samples in the moderately polluted state and the moderately to strongly polluted state was 14.2% and 5.3%.
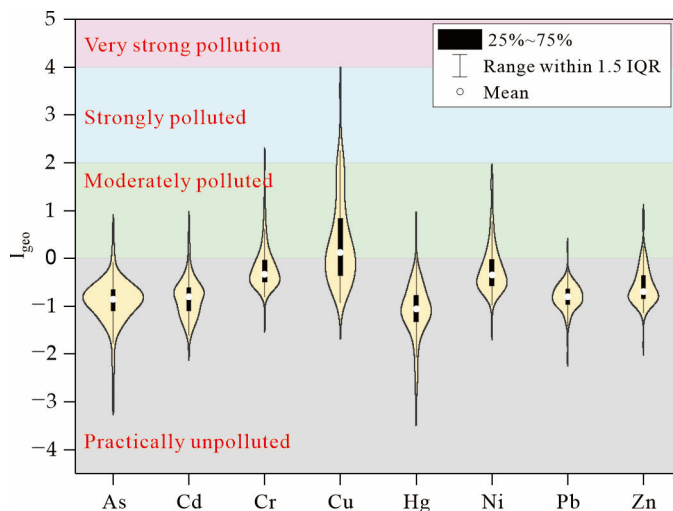
Figure 2. Distribution of the geoaccumulation indexes of heavy metals in the soils.

3.3. Geochemical Speciation of Cu

The geochemical speciation of Cu in soils and tailings is presented in Figure 3. The results reveal that the main forms of Cu were the residual fraction, organic bound fraction, and Fe-Mn oxidation fraction. In soils, the average proportion of different forms follows this order: residual fraction > organic bound fraction > Fe-Mn oxidation fraction > humic acid bound fraction > carbonate bound fraction > water-soluble fraction > exchangeable fraction. The proportion of residual fraction ranged from 13.7% to 80.7%, with an average of 55.9%. The average proportions of organic bound fraction and Fe-Mn oxidation fraction were 19.6% and 15.6%, respectively. In the tailings, the average proportions of different forms followed this order: organic bonding fraction > residual fraction > Fe-Mn oxidation fraction > carbonate bonding fraction> humic acid bonding> exchangeable fraction > water-soluble fraction. The range of the proportion of the organic bound fraction was from 34.7% to 74.9%, with an average of 57%. The average proportions of the residual fraction and Fe-Mn oxidation fraction were 20.2% and 13.9%, respectively. The results indicate that in the tailings, regardless of the total concentration of Cu, the organic bound fraction consistently appeared as the dominant form. However, in soils, a higher proportion of organic bound fraction tended to be present in samples with higher total concentrations of Cu.
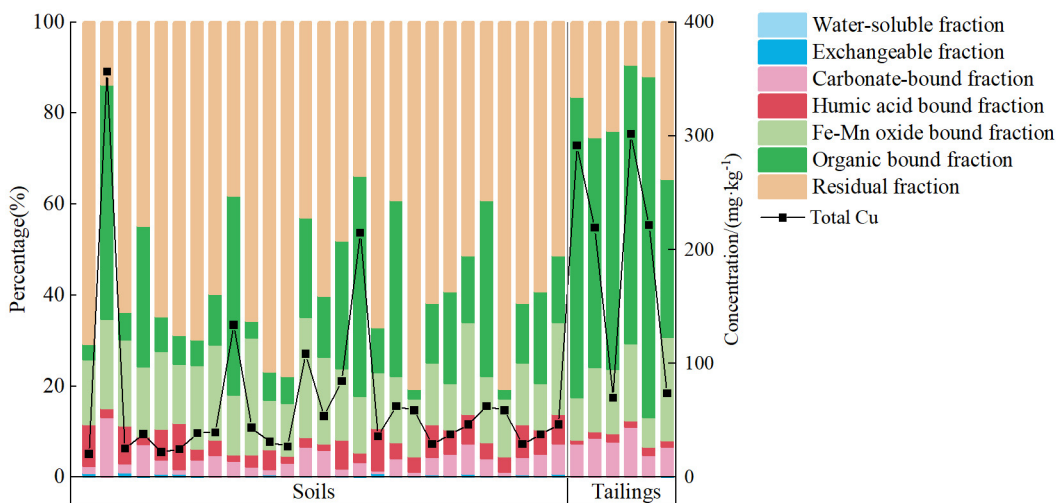

Figure 3. The chemical speciation of Cu in soils and tailings.

3.4. Mineral Composition

The mineral composition of soils, tailings, and stream sediments is presented in Figure 4. The results indicate that the minerals in tailings consisted mainly of diopside and biotite, with an average proportion of 41.9% and 35.9%, respectively. Additionally, the average proportion of amphibole and chlorite was 14.3% and 8.0%. The analysis of the polished section revealed that the diopside rock containing ore minerals consisted of diopside, biotite, amphibole, and opaque minerals. The predominant opaque minerals are likely to be magnetite, chalcopyrite, or pyrite [50]. This suggested that most of the minerals in tailings were inherited from ore-bearing rocks (YS12, diopside rock). Chlorite was primarily the secondary product of weathering for diopside and amphibole. Monzonite and diorite were widely distributed in the study area and serve as the primary parent rock of soils and stream sediments. As a result, soils and stream sediments exhibit a higher proportion of quartz, albite, and biotite compared with the tailings. The average content of quartz, albite, and biotite in soils was 38.6%, 26.9%, and 12.5%, whereas in stream sediments, the average proportion of these minerals was 19.1%, 40.8%, and 23.6%. In the process of weathering, biotite will gradually weather into chlorite or kaolinite, and albite will weather into kaolinite or montmorillonite [63], while quartz has a stronger weathering resistance ability. Compared with the stream sediments, the soils exhibited a higher degree of weathering, resulting in a greater presence of quartz. Conversely, the stream sediments contained more albite and biotite.
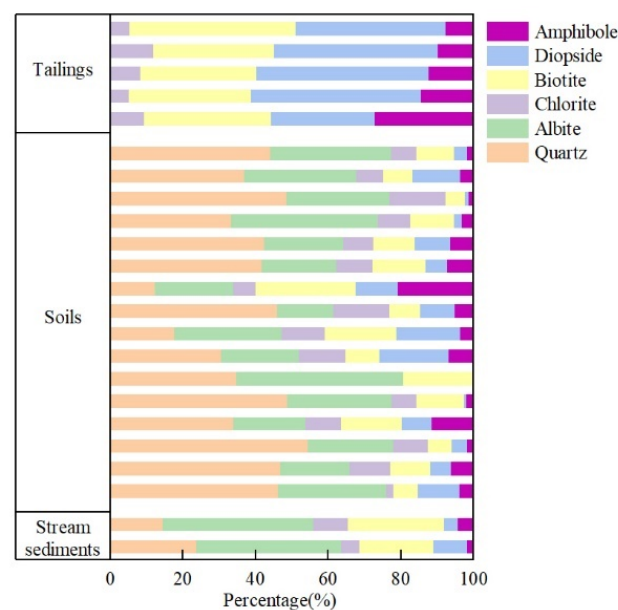

Figure 4. The mineral composition of soils, tailings, and stream sediment samples.

4. Discussion

4.1. Source Identification

The geoaccumulation index of major pollutants from other iron mines in China is presented in Table 7. Cu pollution was not assessed in Hanzhong; however, it was evaluated in Chengde and Ma'anshan. The findings indicated that there was also Cu pollution present in the soils. In comparison with the geoaccumulation index of Cu in the soils from the iron mine in Chengde and Ma'anshan, the geoaccumulation index of Cu in the soil from the study area exhibited a smaller average value and a larger maximum value. This suggested that the extent of Cu pollution in the study area may be relatively lower compared with that of Chengde and Ma'anshan. However, the pollution level at individual sites within the study area may be higher than those found in Chengde and Ma'anshan.

Table 7. Geoaccumulation index of major pollutants from other iron mines in China.

Location	Geoaccumulation Index			Reference
	Element	Range	Average	
Ma'anshan	Cu	−2.67~1.39	0.71	[64]
	Zn	−0.38~1.30	0.38	
	Cd	0.92~4.47	2.79	
Hanzhong	Hg	1.23~3.94	2.67	[65]
	As	−1.28~4.65	1.26	
	Zn	0.65~3.51	0.65	
	Ni	0.06~2.76	0.06	
Chengde	Cu	Approximately 0 to 2.3	1.22	[66]

The results of the characterization of heavy metal and major elements revealed that Cu, Cr, and CaO belong to strong variability, indicating that these elements were extremely unevenly distributed in the soil of the study area. The potential source of elements can be judged by the distribution characteristics of elements. ArcGIS 10.2 software was utilized to create geochemical maps from analysis data of soil, tailings, and stream sediment samples. Inverse distance weighting (IDW) was chosen as the interpolation method. The geochemical distribution of Cu, Cr, and CaO in soils is presented in Figure 5. The rock samples and mining activities can also be observed in Figure 5. The geochemical distribution of Cu and CaO was generally similar, and their distribution is closely related to mining activities, where the soils with high concentrations of Cu and CaO were mainly distributed around the tailings and mining pits. The geochemical distribution of Cr was mainly related to the concentration of rocks, where soils with high concentrations of Cr were distributed around rocks (YS05 and YS10) with high concentrations of Cr.

The concentration of elements was related to the content of minerals, and the content of minerals was determined by parent rock and weathering degree. With the strengthening of weathering, secondary enrichment of stable elements will occur [60,67]. In order to avoid the influence of secondary enrichment on the analysis results, reference elements were used [68]. In the parent rock, Al_2O_3 is mainly enriched in aluminosilicate minerals (albite) and some silicate minerals (such as amphibole and biotite). In general, due to the drought in the study area, albite exhibited strong weathering resistance. Concurrently, the weathering products of these Al_2O_3-rich silicate minerals were clay minerals such as chlorite, kaolinite, and illite [63], all of which were rich in Al_2O_3. Therefore, Al_2O_3 was very stable in the weathering process. In the process of mining, the ore-bearing rock is crushed into debris, magnetite is selected from the debris by a magnetic separator, and the residue is the tailings. There was also no loss of Al_2O_3 in this process. So Al_2O_3 can be a reference element to characterize the concentration of Cu in the original material. The concentration of CaO in the study area was related to the proportion of diopside and amphibole. As weathering intensifies, these minerals are weathered into chlorite, and CaO leaching loss will occur with the dissolution of rainfall. So, CaO can be used as an indicator of weathering degree. The relationship between the values of Cu/Al_2O_3 and the concentrations of CaO in rocks, tailings, and polluted and unpolluted soils in the study area is presented in Figure 6a. The results reveal that, except for ore-bearing rock, the values of Cu/Al_2O_3 in other rocks were relatively low. The values of unpolluted soils were generally lower than those of polluted soils, which were similar to most rocks. This suggested that the Cu in the unpolluted soil was mostly inherited from the weathering of the parent rock, although the degree of weathering is different. The value of Cu/Al_2O_3 in ore-bearing rock reached 51.8, significantly higher than that in other rocks. The value of Cu/Al_2O_3 in tailings ranged from 30.0 to 56.1, with an average value of 46.6, which was close to that in ore-bearing rock, indicating that the high concentration of Cu in tailings was mainly inherited from ore-bearing rock. At the same time, there was a high concentration of CaO in the tailings. As shown in Figure 4, there was also a high proportion of diopside, which was easily weathered under the influence of supergene geochemistry. This indicates that

the degree of weathering in the tailings was low. The high value of Cu/Al_2O_3 was often accompanied by a high concentration of CaO in the polluted soils this feature was very consistent with the tailings. This suggested that the Cu in the polluted soil was affected by tailings.
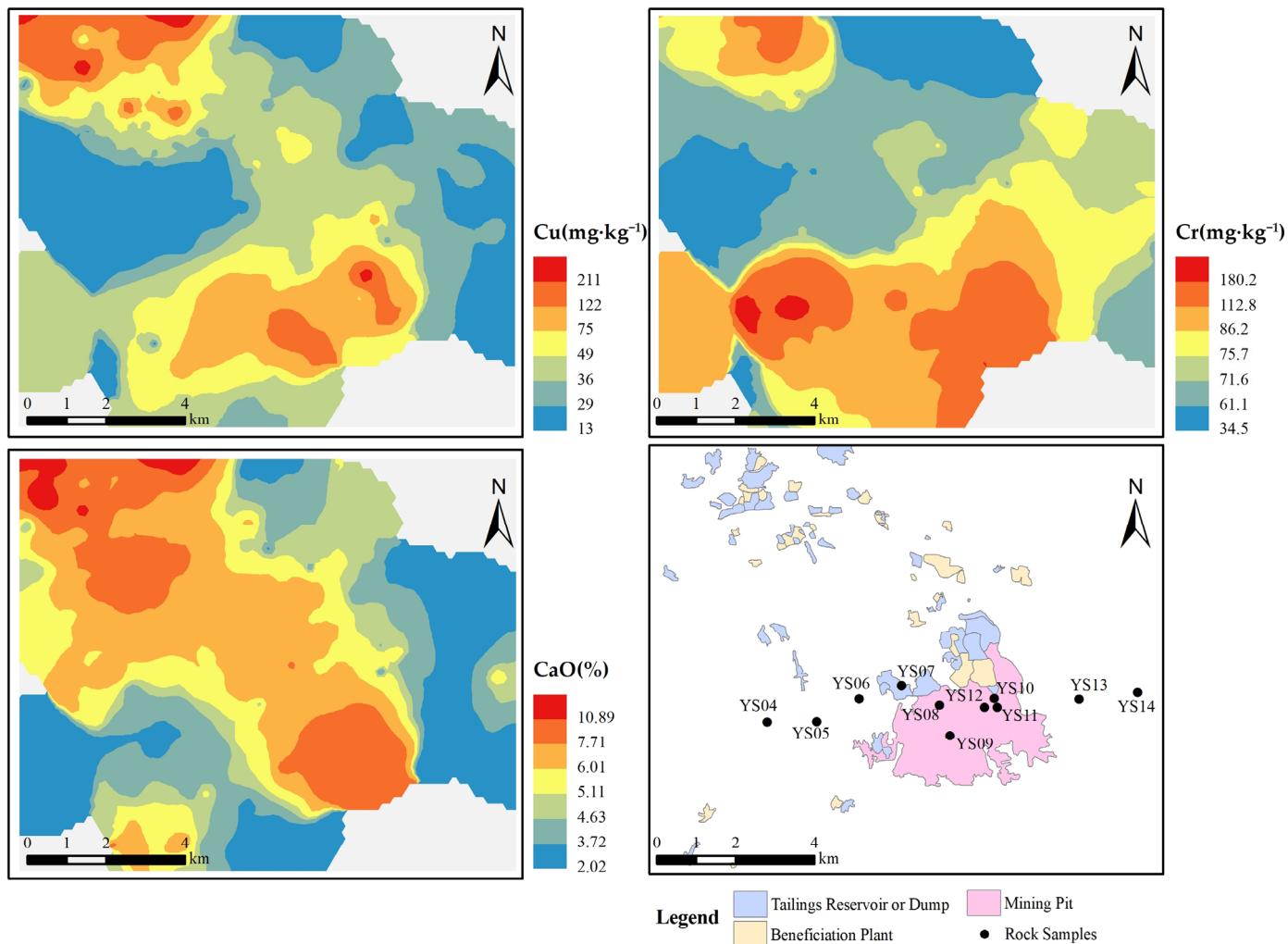

Figure 5. The relationship between geochemical maps of Cu, Cr, and CaO with the distribution of rocks and mining activities.

In general, the CIA is influenced by climatic conditions. Under the same climatic conditions, the CIA of surface soil is often higher than that of deep soil [69]. The CIA and concentrations of total Cu in the soil profile in the study area are presented in Figure 6b. The results reveal that the concentration of Cu in the leached layer (PM-A, 0~20 cm) was significantly higher than that in the illuvial layer (PM-B, 80~100 cm) and parent material layer (PM-C, 200–220 cm), and the concentration of Cu in the parent material layer and illuvial layer was generally close. From the parent material layer to the illuvial layer, the value of CIA increased, while from the illuvial layer to the material layer, the value of CIA decreased. The mineral composition of the soil profile is presented in Table 8. The minerals in the parent material layer were mainly composed of albite. From the parent material layer to the illuvial layer, the concentration of albite decreased, and the concentration of Mg-Fe minerals such as biotite and amphibole also decreased. If not affected by human activities, the proportion of minerals such as amphibole and biotite will continue to decrease from the illuvial layer to the leached layer. But the result was that amphibole and biotite increased and diopside appeared, which was not contained in the parent material layer. The results

reveal that there was an input of exogenous substances in the surface soil, which should be the tailings because of the similar mineral composition to tailings. As presented in Figure 3, the tailings contained a high proportion of organic bound fraction for Cu, which can be utilized to identify their source. The concentrations of organic bound fraction in the soil profile are presented in Figure 6b. The results reveal that the proportions of organic bound fraction Cu in the illuvial layer and parent material layer soil were very low, but they reached 55.4% in the leached layer, indicating that the tailings were the main source of Cu pollution in the surface soil of the study area.
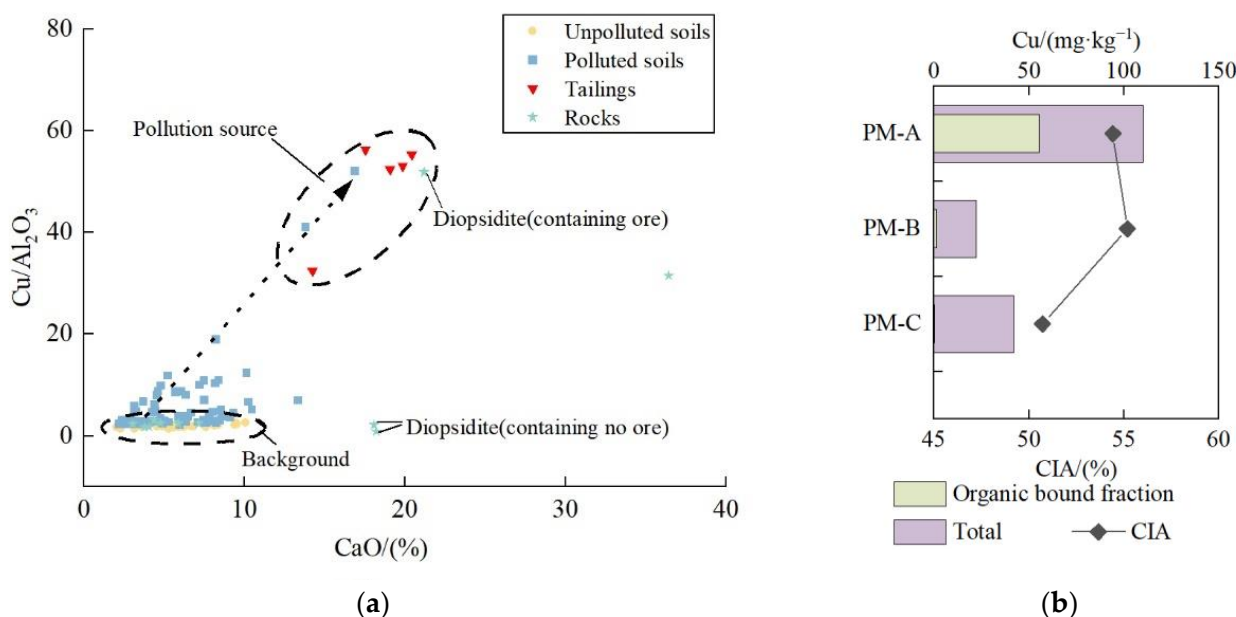

Figure 6. (**a**) The relationship between the values of Cu/Al_2O_3 with the concentrations of CaO in rocks, tailings, polluted and unpolluted soils; (**b**) the concentrations of total and organic bound fraction Cu with the CIA in soil profile.

Table 8. The mineral composition of the soil profile.

	Amphibole	Albite	Chlorite	Quartz	Biotite	Orthoclase	Diopside
PM-A	12.23	34.54	8.34	12.27	14.48	14.56	3.59
PM-B	3.46	33.65	5.85	27.61	4.56	24.87	0
PM-C	9.96	53.63	0.91	7.44	11.56	16.5	0

4.2. Migration Pathways

During the process of mineral processing, the crushed ore was mixed with water, and magnetite was separated from it using a magnetic separator. Subsequently, the water and waste residue were jointly discharged into the tailings reservoir. The water used in the process primarily came from groundwater and water in the tailings reservoir, without adding other chemical reagents. The chemical speciation of Cu is presented in Figure 3, and the results reveal that the concentrations of water-soluble and exchangeable fractions in soils and tailings were very low. These forms of Cu basically represent the part of dissolution migration that can occur in the process of mineral processing and storage of tailings [70], indicating that Cu rarely migrated in the pathway of dissolution in the study area.

According to the announcement made by the Baotou Water Bureau, water erosion was identified as the predominant form of soil erosion in Baotou City, while wind erosion is also widespread. The area of soil erosion in Baotou City is 16,183.13 km², accounting for 58.5% of the land area. The concentrations of Cu in the stream sediments in the study

area are presented in Figure 7a. The samples S01, S02, and S05 were collected from the tributaries located outside the mining area, upstream of the major water system. In contrast, the samples S03, S04, S06, S07, S08, and S09 were collected from the tributaries within the mining area. The results reveal that the concentrations of Cu in the stream sediments located in the mining area were significantly higher than those in the upstream. When the stream system flowing out of the mining area met the stream river system, the concentration of Cu slightly increased, such as S10. The concentrations of Cu in most of the downstream sediments were low, while the samples with high concentrations were always close to the tailings dump. The Cu concentration of S13 was the highest, reaching 140 mg·kg^{-1}. Figure 7b shows that the tailings dump adjacent to S13 was significantly taller than the stream and lacked any enclosure. Therefore, tailings were susceptible to water erosion and deposition into stream sediment. The variation in the concentration of CaO in stream sediments was similar to that of Cu, which is consistent with the element characteristics of the tailings. This suggested that Cu will migrate alongside the transport of the tailings, with hydraulic transport being one of the primary migration pathways.
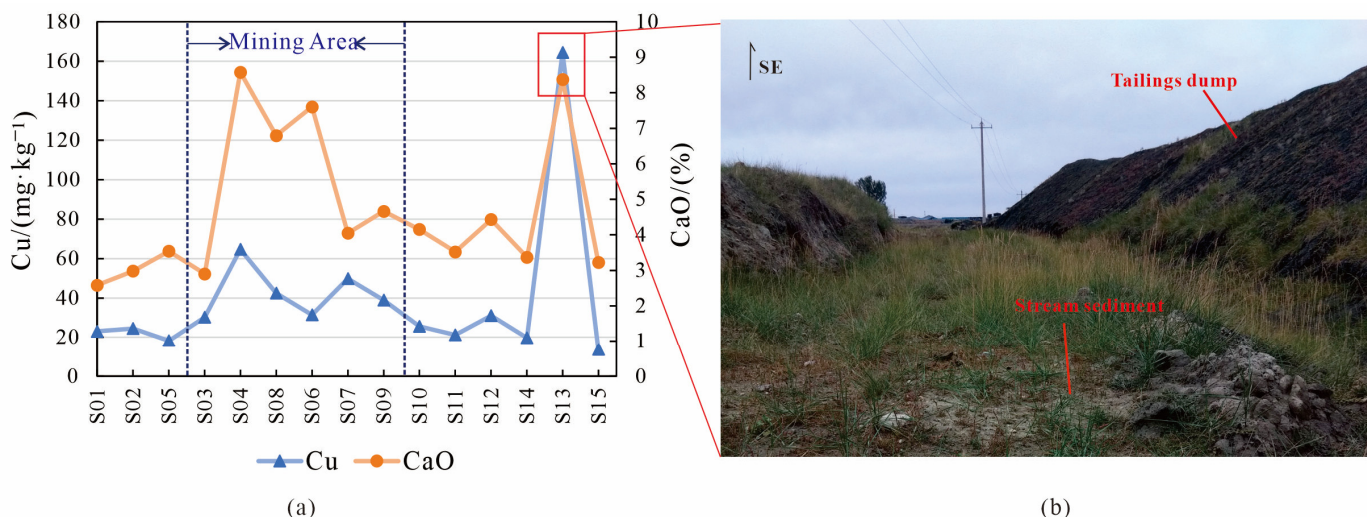

(a)

(b)

Figure 7. (**a**) The concentrations of Cu and CaO in the stream sediments. (**b**) Photo of the surrounding environment of S13.

The annual flux of heavy metals in atmospheric depositions was calculated and is presented in Table 9. The results reveal that the annual fluxes of Cu in atmospheric deposition at Erxianggong, Xiwang Aluminum, and Yinhao exceeded the average value of China, as cited in "Specification of land quality geochemical assessment" (DZ/T 0295-2016) [71]. However, Cd and Hg were significantly lower than the average value. The average value of China was calculated from 1450 samples collected from the agricultural areas of 21 provinces in China. These samples were primarily located in the central and eastern regions of the country. Human activities are more prevalent in these areas compared with the study region. Cd and Hg were mainly associated with industrial activities, coal combustion, and gasoline combustion [27,46]. Therefore, the fluxes of Cd and Hg in atmospheric deposition in the study area were generally lower than the average value of China. In addition to the obvious industrial activities near the Xiwang Aluminum, there were few human activities in the study area, so Cu in the atmospheric deposition of Yinhao and Erxianggong may be mainly derived from dust. PM$_{10}$ was the primary pollutant of air pollution in Baotou City, accounting for more than 70% of the total pollution days [72]. The vegetation coverage of the tailings reservoir and tailings dump in the study area was significantly low. During winter and spring, the surface was dry with high winds, making it easy for the tailings to generate dust and migrate to the surrounding soil, or even further away [73]. Therefore, the annual fluxes of Cu in atmospheric depositions at Erxianggong, Xiwang Aluminum, and Yinhao, around the tailings reservoir and tailings dump, were

higher than the average value of China. This suggested that wind migration was also one of the main migration pathways in the study area.

Table 9. Annual flux of heavy metals in atmospheric depositions.

	As	Cr	Cu	Pb	Cd	Hg
	mg·(m²·a)⁻¹				μg·(m²·a)⁻¹	
Atashan	3.33	15.91	11.69	18.42	238.10	10.01
Liusangou	1.27	8.50	8.30	3.88	58.45	7.73
Yinhao	2.21	15.52	14.16	5.89	64.04	8.28
Xiwang Aluminum	4.76	30.89	19.41	38.13	173.68	17.86
Erxianggong	1.90	13.12	18.67	5.08	61.69	9.36
Average value of China	2.45	15.08	13.09	22.99	482.17	36.03

5. Conclusions

In this paper, the iron mine in Baotou City was selected as the study area, the concentration of heavy metals with major elements, mineral compositions, and heavy metal speciation was measured, and the source and migration pathways were analyzed. The following conclusions can be drawn:

(1) The average concentrations of Cu in the soils, tailings, and stream sediments were higher than the background value. A total of 61.9% of soils are polluted, and the unpolluted to moderately polluted state was the main pollution level.

(2) The tailings were mainly composed of diopside, biotite, and amphibole, while soils were mainly composed of quartz, albite, and biotite. In tailings, the organic bound fraction was always the dominant form, while in soils, the residual fraction was the dominant form. The differences in mineral composition and chemical speciation between tailings and soils can be used to identify the source of Cu.

(3) The high value of Cu/Al_2O_3 and concentration of CaO in polluted soils, tailings, and ore-bearing rock indicated that tailings may be the source of Cu pollution. The variation in CIA value, mineral composition, and the form of Cu in the soil profile can also serve as evidence to support the possibility that Cu pollution in the topsoil originated from tailings.

(4) The migration pathways of Cu might be mainly hydraulic transport and wind transport.

These conclusions indicate that in order to effectively control soil pollution at its source, it is imperative to prevent the leakage of tailings.

Author Contributions: Conceptualization, C.W. and Y.L.; methodology C.W., D.X. and S.Z.; resources, Y.L. writing—original draft preparation, C.W. and D.X.; writing—review and editing, C.W., D.X., Y.L., W.Z., P.B. and S.Z.; project administration, Y.L., W.Z., P.B. and S.Z. All authors have read and agreed to the published version of the manuscript.

Data Availability Statement: No new data were created or analyzed in this study. Data sharing is not applicable to this article.

Conflicts of Interest: The authors declare no conflicts of interest.

References

1. Wu, C.; Zhang, Y.; Zhang, J.; Chen, Y.; Duan, C.; Qi, J.; Cheng, Z.; Pan, Z. Comprehensive evaluation of the eco-geological environment in the concentrated mining area of mineral resources. *Sustainability* **2022**, *14*, 6808. [CrossRef]
2. Strzałkowski, P.; Litwa, P. Environmental protection problems in the areas of former mines with emphasis on sinkholes: Selected examples. *Int. J. Environ. Sci. Technol.* **2020**, *18*, 771–780. [CrossRef]
3. Mestanza-Ramón, C.; Ordoñez-Alcivar, R.; Arguello-Guadalupe, C.; Carrera-Silva, K.; D'Orio, G.; Straface, S. History, Socioeconomic Problems and Environmental Impacts of Gold Mining in the Andean Region of Ecuador. *Int. J. Environ. Res. Public Health* **2022**, *19*, 1190. [CrossRef] [PubMed]

4.   Yan, B.; Liu, J.; Qi, Q.; Liu, W.; Li, X. Study on chain relationship and risk assessment model of coal mine geological disasters. *Arab. J. Geosci.* **2022**, *15*, 900. [CrossRef]

5.   Zhang, D.; Feng, D.; Muzammal, M. Mine Geological Disaster Risk Assessment and Management Based on Multisensor Information Fusion. *Mob. Inf. Syst.* **2022**, *2022*, 1757026. [CrossRef]

6.   Pecina, V.; Juřička, D.; Hedbávný, J.; Klimánek, M.; Kynický, J.; Brtnický, M.; Komendová, R. The impacts of mining on soil pollution with metal(loid)s in resource-rich Mongolia. *Sci. Rep.* **2023**, *13*, 2763. [CrossRef]

7.   Buch, A.C.; Sims, D.B.; de Ramos, L.M.; Marques, E.D.; Ritcher, S.; Abdullah, M.M.S.; Silva-Filho, E.V. Assessment of environmental pollution and human health risks of mine tailings in soil: After dam failure of the Córrego do Feijão Mine (in Brumadinho, Brazil). *Environ. Geochem. Health* **2024**, *46*, 72. [CrossRef] [PubMed]

8.   Kumar, S.; Banerjee, S.; Ghosh, S.; Majumder, S.; Mandal, J.; Roy, P.K.; Bhattacharyya, P. Appraisal of pollution and health risks associated with coal mine contaminated soil using multimodal statistical and Fuzzy-TOPSIS approaches. *Front. Environ. Sci. Eng.* **2024**, *18*, 60. [CrossRef]

9.   Rouhani, A.; Skousen, J.; Tack, F.M.G. An Overview of Soil Pollution and Remediation Strategies in Coal Mining Regions. *Minerals* **2023**, *13*, 1064. [CrossRef]

10. Yu, T.; Jiang, T.; Liu, X.; Ma, X.; Yang, Z.; Hou, Q.; Xia, X.; Li, F. Research progress in current status of soil heavy metal pollution and analysis technology. *Geol. China* **2021**, *48*, 460–476. [CrossRef]

11. Hamada, N.H.S.; Ali, R.A.S.; El-Tabakh, M.A.M.; Bream, A.S. Environmental monitoring: Tobara fish as bioindicators of heavy metal pollution in a coastal ecosystem. *Reg. Stud. Mar. Sci.* **2024**, *69*, 103335. [CrossRef]

12. Saidon, N.B.; Szabó, R.; Budai, P.; Lehel, J. Trophic transfer and biomagnification potential of environmental contaminants (heavy metals) in aquatic ecosystems. *Environ. Pollut.* **2024**, *340*, 122815. [CrossRef]

13. Tumanyan, A.F.; Seliverstova, A.P.; Zaitseva, N.A. Effect of Heavy Metals on Ecosystems. *Chem. Technol. Fuels Oils* **2020**, *56*, 390–394. [CrossRef]

14. Zeng, X.; Liu, D.; Wu, Y.; Zhang, L.; Chen, R.; Li, R.; Gu, W.; Zhang, L.; Liu, C.; Sun, Q. Heavy metal risk of disposable food containers on human health. *Ecotoxicol. Environ. Saf.* **2023**, *255*, 114797. [CrossRef]

15. Mahmoud, N.; Al-Shahwani, D.; Al-Thani, H.; Isaifan, R.J. Risk Assessment of the Impact of Heavy Metals in Urban Traffic Dust on Human Health. *Atmosphere* **2023**, *14*, 1049. [CrossRef]

16. Wang, W.; Zhao, Y.; Ma, Y.; Guo, C.; Jia, J. An Assessment Framework for Human Health Risk from Heavy Metals in Coal Chemical Industry Soils in Northwest China. *Sustainability* **2023**, *15*, 14768. [CrossRef]

17. Panqing, Y.; Abliz, A.; Xiaoli, S.; Aisaiduli, H. Human health-risk assessment of heavy metal–contaminated soil based on Monte Carlo simulation. *Sci. Rep.* **2023**, *13*, 7033. [CrossRef]

18. Wen, Y.; Wang, Y.; Ji, W.; Wei, N.; Liao, Q.; Huang, D.; Meng, X.; Song, Y. Influencing Factors of Elevated Levels of Potentially Toxic Elements in Agricultural Soils from Typical Karst Regions of China. *Agronomy* **2023**, *13*, 2230. [CrossRef]

19. Wen, Y.; Wang, Y.; Tao, C.; Ji, W.; Huang, S.; Zhou, M.; Meng, X. Bioavailability of Cd in Agricultural Soils Evaluated by DGT Measurements and the DIFS Model in Relation to Uptake by Rice and Tea Plants. *Agronomy* **2023**, *13*, 2378. [CrossRef]

20. Kumar, M.; Seth, A.; Singh, A.K.; Rajput, M.S.; Sikandar, M. Remediation strategies for heavy metals contaminated ecosystem: A review. *Environ. Sustain. Indic.* **2021**, *12*, 100155. [CrossRef]

21. Zaka, S.; Aqeel, M.; Mahmood, A.; Noman, A.; Rizvi, Z.F.; Sarfraz, W.; Nazir, A.; Arshad, K.; Khalid, N. Integrative Evaluation of the Ecological Hazards by Microplastics and Heavy Metals in Wetland Ecosystem. *Bull. Environ. Contam. Toxicol.* **2023**, *110*, 81. [CrossRef]

22. Hou, C.; Feng, C.; Liu, S. *Distribution, Risk Evaluation, and Source Analysis of the Heavy Metals in the Sediment Deposition of the Lower Shichuanhe River*; Acta Geochimica: Shaanxi, China, 2023; Volume 42, pp. 832–844.

23. Xie, S.; Lan, T.; Xing, A.; Chen, C.; Meng, C.; Wang, S.; Xu, M.; Hong, M. Spatial distribution and ecological risk of heavy metals and their source apportionment in soils from a typical mining area, Inner Mongolia, China. *J. Arid Land* **2023**, *5*, 1196–1215. [CrossRef]

24. Mostafa, M.T.; El-Nady, H.; Gomaa, R.M.; Abdelgawad, H.F.; Abdelhafiz, M.A.; Salman, S.A.E.; Khalifa, I.H. Urban geochemistry of heavy metals in road dust from Cairo megacity, Egypt: Enrichment, sources, contamination, and health risks. *Environ. Earth Sci.* **2023**, *83*, 37. [CrossRef]

25. Tang, X.-F.; Wu, Y.; Han, L.-B.; Lan, Z.; Rong, X.-P. Characteristics of heavy metal migration in farmland. *Environ. Earth Sci.* **2022**, *81*, 338. [CrossRef]

26. Li, C.; Li, M.; Zeng, J.; Yuan, S.; Luo, X.; Wu, C.; Xue, S. Migration and distribution characteristics of soil heavy metal (loid)s at a lead smelting site. *J. Environ. Sci.* **2024**, *135*, 600–609. [CrossRef]

27. Qin, M.; Jin, Y.; Peng, T.; Zhao, B.; Hou, D. Heavy metal pollution in Mongolian-Manchurian grassland soil and effect of long-range dust transport by wind. *Environ. Int.* **2023**, *177*, 108019. [CrossRef]

28. Bux, R.K.; Batool, M.; Shah, S.M.; Solangi, A.R.; Shaikh, A.A.; Haider, S.I.; Shah, Z.-u.-H. Mapping the Spatial distribution of Soil heavy metals pollution by Principal Component Analysis and Cluster Analyses. *Water Air Soil Pollut.* **2023**, *234*, 330. [CrossRef]

29. Liu, J.; Kang, H.; Tao, W.; Li, H.; He, D.; Ma, L.; Tang, H.; Wu, S.; Yang, K.; Li, X. A spatial distribution—Principal component analysis (SD-PCA) model to assess pollution of heavy metals in soil. *Sci. Total Environ.* **2023**, *859*, 160112. [CrossRef]

30. Aidoo, E.N.; Appiah, S.K.; Awashie, G.E.; Boateng, A.; Darko, G. Geographically weighted principal component analysis for characterising the spatial heterogeneity and connectivity of soil heavy metals in Kumasi, Ghana. *Heliyon* **2021**, *7*, e08039. [CrossRef]

31. Zhang, S.; Wang, C.; Liu, J.; Xing, Y.; Liu, Q.; Liu, J.; Liu, F. Assessment of Heavy Metal Pollution and Ecological Risk in Soils of the Southwestern Part of the Xiongan New Area. *Earth Sci. Front.* **2021**, *28*, 238–249.

32. Liu, P.; Wu, Q.; Hu, W.; Tian, K.; Huang, B.; Zhao, Y. Effects of atmospheric deposition on heavy metals accumulation in agricultural soils: Evidence from field monitoring and Pb isotope analysis. *Environ. Pollut.* **2023**, *330*, 121740. [CrossRef] [PubMed]

33. Ning, Y.; Yang, B.; Yang, S.; Ye, J.; Li, J.; Ren, L.; Liu, Z.; Bi, X.; Liu, J. Application of Pb Isotopes and REY Patterns in Tracing Heavy Metals in Farmland Soils from the Upper-Middle Area of Yangtze River. *Int. J. Environ. Res. Public Health* **2023**, *20*, 966. [CrossRef] [PubMed]

34. Yu, E.; Liu, H.; Dinis, F.; Zhang, Q.; Jing, P.; Liu, F.; Ju, X. Contamination Evaluation and Source Analysis of Heavy Metals in Karst Soil Using UNMIX Model and Pb-Cd Isotopes. *Int. J. Environ. Res. Public Health* **2022**, *19*, 12478. [CrossRef] [PubMed]

35. Yao, C.; Shen, Z.; Wang, Y.; Mei, N.; Li, C.; Liu, Y.; Ma, W.; Zhang, C.; Wang, D. Tracing and quantifying the source of heavy metals in agricultural soils in a coal gangue stacking area: Insights from isotope fingerprints and receptor models. *Sci. Total Environ.* **2023**, *863*, 160882. [CrossRef] [PubMed]

36. Chen, Z.; Ding, Y.; Jiang, X.; Duan, H.; Ruan, X.; Li, Z.; Li, Y. Combination of UNMIX, PMF model and Pb-Zn-Cu isotopic compositions for quantitative source apportionment of heavy metals in suburban agricultural soils. *Ecotoxicol. Environ. Saf.* **2022**, *234*, 113369. [CrossRef] [PubMed]

37. Liu, L.; Xu, X.; Han, J.; Zhu, J.-M.; Li, S.; Liang, L.; Wu, P.; Wu, Q.; Qiu, G. Heavy metal(loid)s in agricultural soils in the world's largest barium-mining area: Pollution characteristics, source apportionment, and health risks using PMF model and Cd isotopes. *Process Saf. Environ. Prot.* **2022**, *166*, 669–681. [CrossRef]

38. Han, Y.; Hu, Y.; Qang, Q.; Shi, M.; Zhou, L. Progress of copper isotope and its application in environmental pollution tracing. *Bull. Geol. Sci. Technol.* **2023**, *42*, 378–387.

39. Wang, L.; Jin, Y.; Weiss, D.J.; Schleicher, N.J.; Wilcke, W.; Wu, L.; Guo, Q.; Chen, J.; O'Connor, D.; Hou, D. Possible application of stable isotope compositions for the identification of metal sources in soil. *J. Hazard. Mater.* **2021**, *407*, 124812. [CrossRef]

40. Zhang, M.; Song, H.; Shang, J.; Liu, X.; Qi, S.; Li, H. Spectroscopic methods for isotope analysis of heavy metal atoms: A review. *Spectrochim. Acta Part B At. Spectrosc.* **2023**, *207*, 106740. [CrossRef]

41. Madadi, R.; Mejjad, N.; De-la-Torre, G.E. Geochemical speciation, ecological risk, and source identification of heavy metal(loid)s in sediments and waters from Musa Estuary, Persian Gulf. *Mar. Pollut. Bull.* **2023**, *190*, 114836. [CrossRef]

42. Chen, X.; Wu, P.; Chen, X.; Liu, H.; Li, X. Source apportionment of heavy metal(loid)s in sediments of a typical karst mountain drinking-water reservoir and the associated risk assessment based on chemical speciations. *Environ. Geochem. Health* **2023**, *45*, 7585–7601. [CrossRef]

43. Chen, B.; He, R.; Cai, P.; Huang, G.; Wang, F. Geochemical Speciation, Risk Assessment, and Sources Identification of Heavy Metals in Mangrove Surface Sediments from the Nanliu River Estuary of the Beibu Gulf, China. *Sustainability* **2022**, *14*, 9112. [CrossRef]

44. Cheng, L.; Ning, X. The assessment of social progress index in the eco-city construction for Baotou. *J. Arid. Land Resour. Environ.* **2014**, *28*, 12–16. [CrossRef]

45. Bai, Y.; Li, Y.; Fang, L. The current situation and prevention proposals of the mine geological environment in Baotou city. *China Min. Mag.* **2020**, *29*, 114–116.

46. Guo, W.; Zhao, R.; Zhang, J.; Bao, Y.; Wang, H.; Yang, M.; Sun, X.; Jin, K. Distribution characteristic and assessment of soil heavy metal pollution in the iron mining of Baotou in Inner Mongolia. *Environ. Sci.* **2011**, *32*, 3099–3105.

47. Wang, C.; Li, Y.; Zhou, W.-h.; Mao, L.; Lu, Z.; Hu, H.; Du, X.; Bian, P.; Gao, Q. Determination and health hazard assessment of multi-element in soils from Guyang County, Baotou City. *Rock Miner. Anal.* **2022**, *41*, 476–487. [CrossRef]

48. Zhao, T.; Liu, Y.; Deng, Y.; Wang, G. Progress and Prospect of Mine Ecological Restoration in China. *J. Resour. Ecol.* **2023**, *4*, 681–682.

49. Hao, G.; Wang, H.; Niu, G.; Kang, J.; Hao, S. Metamorphic geotectonic research and scientific significance in China. *Geol. Surv. Res.* **2020**, *43*, 89–96.

50. Liu, F.; Su, S.; Yu, X.; Liang, F.; Hu, Y.; Niu, X. Characteristics and petrogenesis of zoned amphiboles in Wengeqi mafic-ultramafic complex, Inner Mongolia. *Earth Sci. Front.* **2013**, *20*, 206–222. [CrossRef]

51. Gao, Z.; Wang, L.; Gao, L. Chemical characteristics and source apportionment of atmospheric precipitation in Baotou urban area. *Environ. Chem.* **2024**, *43*, 1–14.

52. Wang, J.; Zuo, L.; Li, Z.; Mu, H.; Zhou, P.; Yang, J.; Zhao, Y.; Qin, K. A detection method of trace metal elements in black soil based on hyperspectral technology: Geological implications. *J. Geomech.* **2021**, *27*, 418–429.

53. Wu, C.; Sun, B.; Tian, M.; Cheng, X.; Liu, D.; Zhou, Y. Enrichment Characteristics and Ecological Risk Assessment of Heavy Metals in a Farmland System with High Geochemical Background in the Black Shale Region of Zhejiang, China. *Minerals* **2024**, *14*, 375. [CrossRef]

54. Liu, Y.; Wang, W.; Dong, L. XRD Bulk Mineral Distribution Patterns of Surface Sediments in the Western Arctic Ocean and Bering Sea. *Acta Sedimentol. Sin.* **2023**, *41*, 1054–1066.

55. Zhang, G.; Chen, S.; Long, R.; Ma, B.; Chang, Y.; Mao, C. Distribution of Heavy Metals in Surface Sediments of a Tropical Mangrove Wetlands in Hainan, China, and Their Biological Effectiveness. *Minerals* **2023**, *13*, 1476. [CrossRef]

56. Wang, X.; Huang, Z.; Su, M.; Li, S.; Wang, Z.; Zhao, S.; Zhang, Q. Characteristics of reference and background values of soils in Hetao area. *Rock Miner. Anal.* **2007**, *26*, 287–292. [CrossRef]

57. Müller, G. Index of geoaccumulation in sediments of the Rhine River. *GeoJournal* **1969**, *2*, 108–118.

58. Nasir, M.J.; Wahab, A.; Ayaz, T.; Khan, S.; Khan, A.Z.; Lei, M. Assessment of heavy metal pollution using contamination factor, pollution load index, and geoaccumulation index in Kalpani River sediments, Pakistan. *Arab. J. Geosci.* **2023**, *16*, 143. [CrossRef]

59. Huang, X.; Fu, Q.; Wang, J. Distribution and Pollution Assessment by Index of Geoaccumulation about the Heavy Metals in Sediments of Dexing Copper Mine Rainwater Network. *IOP Conf. Ser. Earth Environ. Sci.* **2020**, *455*, 012186. [CrossRef]

60. Négrel, P.; Ladenberger, A.; Reimann, C.; Demetriades, A.; Birke, M.; Sadeghi, M.; Albanese, S.; Andersson, M.; Baritz, R.; Batista, M.J.; et al. GEMAS: Chemical weathering of silicate parent materials revealed by agricultural soil of Europe. *Chem. Geol.* **2023**, *639*, 121732. [CrossRef]

61. Kalinin, P.I.; Kudrevatykh, I.Y.; Malyshev, V.V.; Pilguy, L.S.; Buhonov, A.V.; Mitenko, G.V.; Alekseev, A.O. Chemical weathering in semi-arid soils of the Russian plain. *Catena* **2021**, *206*, 105554. [CrossRef]

62. *GB15618-2018*; Soil Environmental Quality—Risk Control Standard for Soil Contamination of Agricultural Land. Ministry of Ecology and Environment of the People's Republic of China: Beijing, China, 2018.

63. Li, F.; Li, S.; Yang, Y.; Cheng, L. Advances in the study of weathering products of primary silicate minerals, exemplified by mica and feldspar. *Acta Petrol. Mineral.* **2006**, *25*, 440–448.

64. Niu, S.; Fang, Q.; Yu, J.; Wu, J. Heavy Metals Present in the Soils from Extremely Large Opencast Iron Mine Pit. *Bull. Environ. Contam. Toxicol.* **2021**, *107*, 984. [CrossRef] [PubMed]

65. Song, F.; Zhang, X.; Wang, Y.; Li, C.; TANG, B. Heavy Metal Pollution in Soils Surrounding an Iron Tailings in Upstream Areas of Hanjiang River, Shaanxi Province. *J. Agro-Environ. Sci.* **2015**, *9*, 1707–1714.

66. Sun, H.; Wei, X.; Jia, F.; He, Z.; Sun, X. Geochemical baseline and ecological risk accumulation effect of soil heavy metals in the small-scale drainage catchment of V-Ti-magnetite in the Yixun River basin, Chengde. *Acta Geol. Sin.* **2021**, *95*, 588–604.

67. Hasan, O.; Miko, S.; Mesić, S.; Peh, Z. Chemical Weathering Rates of Soils Developed on Eocene Marls and Sandstones in a Mediterranean Catchment (Istria, Croatia). *Land* **2023**, *12*, 913. [CrossRef]

68. Tongggiroh, A.; Imran, A.M.; Haerany, S. Environmental Geochemistry of Heavy Metals and Plagioclase Background Enrichment Factor in Coastal Sediments at Lumpue—Parepare, South Sulawesi, Indonesia. *IOP Conf. Ser. Earth Environ. Sci.* **2019**, *370*, 012002. [CrossRef]

69. Oke, S. Intensity of Chemical Weathering Over Three Meta-igneous Rocks: Importance for Trace Metals Enrichment in Soil Profiles. In *Recent Advances in Environmental Science from the Euro-Mediterranean and Surrounding Regions*, 2nd ed.; EMCEI 2019. Environmental Science and Engineering; Springer: Cham, Germany, 2021; pp. 1287–1291. [CrossRef]

70. Huang, X.; Zhu, X.; Tang, L.; Ji, H.; Jin, Y. Studies on the distribution and chemical speciation of heavy metals in a iron mine soil of the upstream area of Miyun Reservoir, Beijing. *China Environ. Sci.* **2012**, *32*, 1632–1639.

71. *DZ/T 0295-2016*; Specification of Land Quality Geochemical Evaluation. China Geological Survey: Beijing, China, 2016.

72. Zhou, Z.H.; Liu, T.; Dudagula; Ren, L.; He, Z.; Lu, Z.; He, J. Characteristics of Atmospheric Pollutants and Influencing Factors in Baotou. *Res. Environ. Sci.* **2017**, *30*, 202–213. [CrossRef]

73. Cheng, H.; Zhang, K.; Jiang, N.; Zou, X.; Wu, B.; He, W. Dust amoun treaching typical cities from dust emissions due to soil wind erosion in Beijing-Tianjins and storm source regions and its source analysis. *Chin. Sci. Bull.* **2023**, *68*, 801–816. [CrossRef]